EFFECTS OF NEUTRON IRRADIATION ON THE STRUCTURAL PERFORMANCE OF THE CONCRETE BIOLOGICAL SHIELD IN LIGHT WATER REACTORS

Yann M Le Pape[1], Amani Cheniour[1], Mohammed Alnaggar[1], Eva Davidson[1], Yong Joon Choi[2], Samantha Sabatino[1]

[1] Oak Ridge National Laboratory, Oak Ridge TN, USA (lepapeym@ornl.gov)
[2] Idaho National Laboratory, Idaho Falls, ID, USA

ABSTRACT

Long-term operation of light-water reactors includes the assessment of the structural integrity of the concrete biological shield (CBS) exposed in-service to fast neutrons and gamma rays exiting the reactor pressure vessel (RPV). This paper summarizes the methodology for degradation of CBS due to in-service radiation which can be increased by the pressure and thermal shock resulting from LBLOCA. In this study, radiation transport is performed using a VERA-shift model of the reactor core, RPV, and CBS to obtain the fast neutron 3D-fluence fields over time. These serve as inputs for the structural simulations performed using a meso-scale approach with the lattice discrete particles model and a continuum approach using the finite element code Grizzly. Local effects at the reinforcing bars and other metal attachments are not included in this radiation transport model and structural model. Accident conditions during a loss-of-coolant accident (LOCA) are obtained using the code RELAP 5 to estimate the pressure and temperature of the air in the reactor cavity; other LOCA effects are not considered. At mid-elevation of the reactor core, the effects of irradiation cause degradation of the concrete near the cavity. For long term operation, the degraded depth extends beyond the area subject to a fast neutron fluence of 10^{19} n.cm^{-2} (E > 0.1 MeV) and beyond the location of the reinforcement. A simplified axi-symmetric sector model of CBS with liner is used in this study. Local effects at the reinforcing bars and other metal attachments are not included in this radiation transport model and structural model.

INTRODUCTION

In light-water reactors (LWRs), the concrete biological shield (CBS) designates the concrete structure directly facing the reactor pressure vessel (RPV). The CBS's primary function is to protect equipment and personnel from the neutron and gamma radiation exiting the RPV. Neutron and gamma irradiation dose rates are attenuated significantly by the presence of constitutive water. The CBS tends to be more massive in pressurized water reactors (PWRs) than the internal structures in boiling water reactor (BWR) designs because the CBS typically supports the reactor pressure vessel (RPV), and other large equipment. However, the RPV is supported by steel columns embedded in the CBS in some designs. The RPV's supporting structure transfers the static or dynamic load of the reactor to the foundation system. For some cases, RPV support comprises short columns, support beams, and pedestals embedded in the CBS below the nozzles. The beams supporting the girders placed directly below the nozzles are located at the approximate elevation of the top of the fuel assembly. At a projected operation of 80 years, the surface CBS is exposed to the following irradiation conditions: fast neutron flux at ~0.1-0.25 × 10^{11} n.cm^{-2} s^{-1} (E > 0.1MeV), fast neutron fluence at ~2.0-6.0 × 10^{19} n.cm^{-2} (E > 0.1 MeV), gamma dose ~100–400 MGy, and temperature

at < 65 °C (by design). Irradiation affects the physical and structural properties of concrete (Hilsdorf et al, 1978; Field et al., 2015). The main degradation mechanisms are caused by (1) the fast neutron–induced volumetric change of aggregate-forming minerals, most of which are observed at $> 10^{19}$ n.cm^{-2} (E > 0.1 MeV), and (2) the radiolysis-induced dehydration of cementitious hydrates (Denisov et al. 2012). Radiation-induced volumetric expansion (RIVE) may reach several percents, depending on the concrete's chemical composition, the fast neutron fluence, and flux. Elastic modulus, compression, and tensile strength decrease at fluences $> 10^{19}$ n.cm^{-2} (E > 0.1 MeV). In extended nuclear power plant operation, the structural integrity of the CBS to transfer all design basis loadings to the foundation should be assessed using state-ot-the-art simulation tools, coupling the irradiation transport simulation that can capture the important aspects of transport through CBS including the embedded steel. In this paper, the system safety analysis code RELAP5-3D, and two structural analysis codes: namely, the lattice discrete particle model (LDPM), and the finite element (FE) code (Grizzly) have been used. The presented results are based on irradiated concrete properties obtained from published experiments data obtained under accelerated conditions in test reactors.

IRRADIATION TRANSPORT

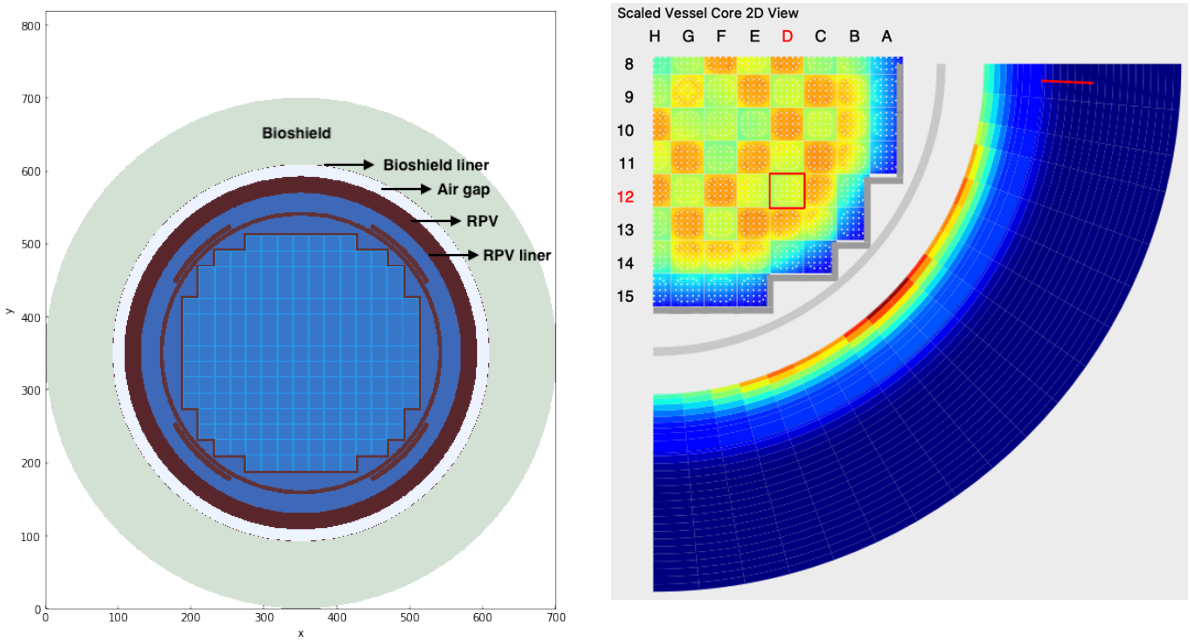

Figure 1. (Left) BN1 VERA model (x-y slice at active core mid-plane). [Note: x-axis in cm and y-axis in cm]; (Right) Cycle 2 radial fluence at z=193.1 cm (after ~1.3 EFPY).

The VERA software suite enables neutron transport calculations using both deterministic and hybrid deterministic / Monte Carlo (MC) methods (Kochunas et al, 2017). High-fidelity in-core radiation transport calculations with temperature feedback are performed using MPACT (Collins et al., 2016), a deterministic neutron transport code, and COBRA-TF (CTF) (Avramova, 2009), a subchannel thermal hydraulics code. This study reuses a previously developed VERA model of a Westinghouse four-loop PWR with a thermal power rating of 3,459 MWh. It should be noted that 4-loop PWRs tend to produce lower fluence at the surface of the CBS than 3-loop and 2-loop plants (Esselman and Bruck, 2018). Hence, the results of this study may not be considered as a bounding data. The reactor core consists of 193 Westinghouse 17 × 17 fuel assemblies. There are eight control rod banks consisting of 57 rod cluster control assemblies (RCCAs) with 24 rodlets in each RCCA (Godfrey et al., 2016). The VERA model also includes in-core instruments that monitor the neutron flux in the reactor. Each cycle in an LWR has a unique fuel loading pattern. The details of the model are presented in Cheniour et al. (2023). Figure 1 (left) shows the model at the core's

mid-plane and the flux map during cycle 2. Figure 5 (d) shows the fluence profiles at 40, 60, and 80 years of operation. For additional details on radiation transport through CBS refer to NUREG/CR 7281.

IN-SERVICE IRRADIATION-INDUCED DEGRADATION

Two simplified structural models were created using an LDPM and an FE model (FEM), Grizzly.

Lattice Discrete Particle Model (LDPM)

The LDPM is a concrete mesoscale discrete model with effective capabilities to model concrete cracking and fracture (Cusatis et al., 2011). Concrete is represented through an assemblage of interacting large aggregate idealized as size-distributed spherical particles that are randomly generated. Particle centers serve as the computational nodes of the system. Particles interact through stress–strain vectors at the centroids of the particles' delimiting facets. These are created using Delaunay tetrahedralization and volume tessellation. Strains are defined from the relative displacement between particle centroids using rigid body kinematics from the nodal displacements and rotations. Vectorial stresses are related to strains via distinctive constitutive relationships that represent (1) cohesion and friction during tension and tension-shear relative deformation, (2) plastic deformation under pure shear, and (3) material compaction and pore collapse under compression and compression shear. The proposed modeling strategy for the CBS is comparable to the rigid body springs network (RBSM) developed by Kambayashi et al. (2020). The main objective of this model is to assess the extent of damage (here represented by cracks, or displacement discontinuities) and to compare this damage depth with the results obtained from the Grizzly FE-based model. Because of computational capability limitations associated with the explicit representation of the aggregate size distribution, the present model is representative of a CBS *sector* approximately facing the RPV belt line where the fast fluence flux is maximal along the vertical direction. Previous studies (Le Pape, 2015; Khmurovska et al., 2019; Kambayashi et al., 2020) have shown that the irradiation-induced degradation may be limited to the first < 500 mm of the CBS radius, the region of the model adjacent to the reactor cavity corresponding to the *meso-scale model domain* (MSMD with explicit representation of the aggregates), whereas the remainder of the sector assumes a *continuum model domain* (CMD). The total thickness of the CBS *sector* is 2 m, and its height is 10 cm (8 times the size of the largest aggregate). The sector is extruded in the orthoradial direction by 4.4 degrees, which corresponds to a dimension of ~20 cm and ~35 cm at the inner radius and outer radius of the sector, respectively. In the MSMD, the aggregate size distribution assumes a Fuller function (coefficient: 0.6) with aggregate sizes ranging from 4 to 13 mm. Although the steel liner may be not designed as a structural member, the model includes a steel liner represented by 5 mm thick 6-node shell elements, as shown in
Figure *2*. The liner' simplified model does not account for the presence of connectors. Thus, the local stress state in the liner and adjacent concrete may not be represented accurately.

To model axisymmetric boundary conditions, two rigid frictionless plates were added along the lateral faces of the MSMD and CMD. The bottom and top surfaces are considered fixed, preventing vertical structural deformation. The CMD remains in the elastic regime. The constitutive model of the concrete in the MSMD includes elasticity, fracture, creep, and RIVE of meta-chert tuff-like 92% quartz-rich aggregate. The fast neutron fluence profile varies only in the radial direction and corresponds to the profile location from which the Grizzly outputs are extracted. For this study, at that specific location, the fast neutron fluence at the surface of the concrete is ~2×10^{19} n.cm^{-2} (E > 10 keV) at 80 years of operation. The temperature profile linearly decreases from 65 °C at the liner to 40 °C at the back of the CMD. Figure 3 shows the local crack opening (color map using a logarithmic scale) observed at the top surface of the MSMD at 40, 60, and 80 years. Radial cracks (i.e., located in $\theta - z$ planes and opening in the radial direction) are present in a region defined approximately between the concrete surface of the reactor cavity and a surface located at a distance of ~+200 mm inside the CBS. Cracking is more important toward the reactor cavity following the RIVE radial profile. The maximum crack opening decreases exponentially with the radius to reach a maximum

crack opening of > 1 mm to <10 µm at a respective depth of 0 to ~200 mm, as shown on the left side of Figure 4. Near the linear interface, the RIVE-induced cracking appears to cause some delamination and spalling. Moving beyond a depth of ~200 mm, cracks with openings below 100 µm are observed. They result from the vertical and orthoradial tensile stresses forming to balance the compression stresses in the region where RIVE is active. Thus, these cracks openings are oriented along the vertical and orthoradial directions.

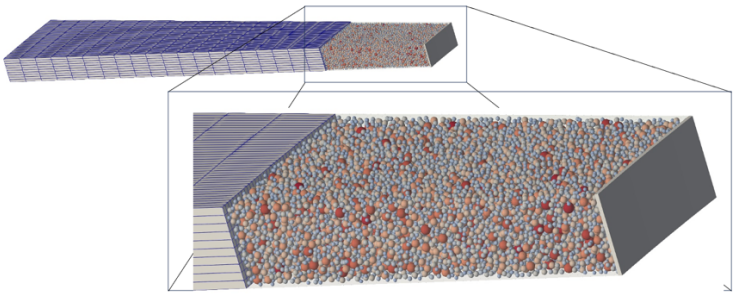

Figure 2. Geometry of the sector model. The left portion (regular mesh) corresponds to the CMD, and the right portion, which was modeled with LDPM, corresponds to the MSMD. The liner is modeled with shell elements.

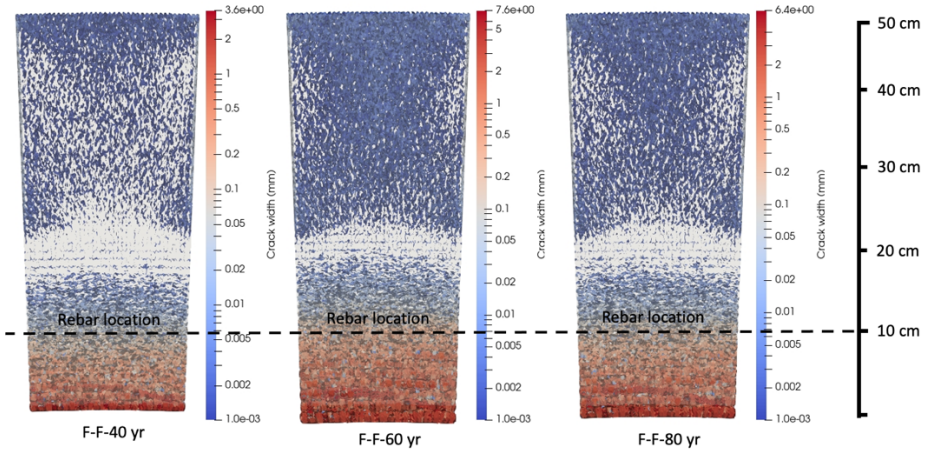

Figure 3. Radial profiles of the maximum crack opening at 40, 60, and 80 years of operation.

To compare the damage profiles derived from the FEM and the crack opening profiles derived from the LDPM simulations, a representative volume of unirradiated concrete under external biaxial loading is modeled separately using LDPM. Such a loading is representative of the irradiation-induced conditions observed near the reactor cavity. It can be observed that the equivalent damage profile drops are much sharper obtained by LDPM analysis than those illustrating the damage obtained by the FE simulations, as shown on the right side of Figure 4. This indicates that the residual strength of the irradiated concrete near the reactor cavity is very limited. However, the extent of the damage profile depth is ~8, 10, and 11 cm at 40, 60, and 80 years, respectively for neutron fluence ~2×10^{19} n.cm^{-2} (E > 10 keV), a corresponding RIVE value of XXX, both calculated at the surface of the concrete.

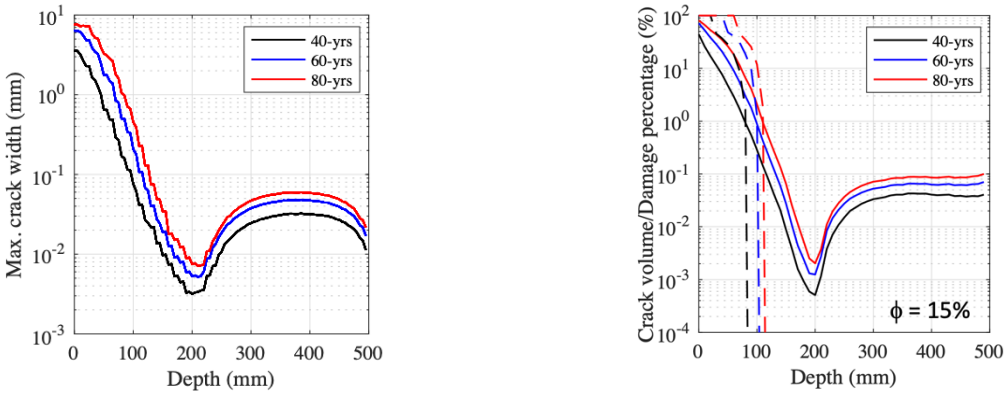

Figure 4. Radial profiles of the maximum crack opening (left), and comparison of the radial profiles of equivalent damage index (dashed lines) and crack volume (solid lines) (right). (ϕ denotes the adopted crack volume threshold causing full damage).

Finite Elements Model (FEM)

In this study, a modified prototypical reactor geometry for a modified Westinghouse 4-loop PWR was adopted. The simulation of CBS was performed using the FE code Grizzly leveraging the multiphysics coupling capabilities provided by MOOSE (Permann et al., 2020). The CBS is idealized as a 2 m thick cylindrical reinforced concrete wall (inner radius: 2.582 m) lined with a 5 mm steel plate facing the reactor cavity. The steel connectors anchoring this liner are not represented (perfect bond condition). The height of the cylindrical section of the reactor is 4.071 m. Vertical and hoop #8 (25.4 mm dia.) reinforcement bars are located at a 76.2 mm depth on the inner and outer sides of the cylindrical wall. The CBS rests on a 2 m thick concrete basemat with fixed boundary conditions, creating strong structural deformation constraints. The FEs are mostly first-order hexahedra. The mesh is refined in the region subject to high fast neutron flux. The reinforcement bars are modeled with truss elements perfectly bonded to the concrete.

Carbon steel liner and reinforcements are assumed to be perfectly elastic. Simulation results show that this hypothesis is correct. The concrete constitutive model includes the following behaviors: thermal expansion, RIVE, shrinkage, and creep. The B3 logarithmic viscoelasticity model (based on the B3 model) (Bažant and Jirasek, 2018) is adopted, and irradiation-induced and structural damage are also included. The acceleration effects of temperature and irradiation on the creep rate are not considered. Thus, the relaxation of RIVE-induced elastic energy in the cement paste is minimized, leading to energy dissipation through cracking. Hence, the approach presented here is considered conservative in terms of the extent of damage propagation through the CBS over prolonged operation. Two sources of damage are considered. First, the *intrinsic irradiation-induced damage* corresponds to the loss of mechanical properties caused by irradiation-induced RIVE as measured from post-irradiation examination and testing on specimens that were not subjected to any mechanical constraints during the irradiation experiment. Second, the *structural damage* corresponds to the nonlinear stress–strain behavior of concrete under loading; in the present case, the nonuniform RIVE field associated with the stiffness of the structure causes internal stresses to form. Both effects are independently modeled and combined, assuming that overall damage is the maximum of these two. The main results of the FE mechanical simulation are as follows.

1. The steel liner and reinforcing bars are subject to compression stresses lower than 40 MPa, well under the yielding stress.
2. The CBS is subject to nonuniform stress fields caused by the nonuniform RIVE profile. Toward the reactor cavity, important biaxial compression stresses (Figure 5c) are created that accentuate the formation of irradiation-induced damage (Figure 5d).
3. The overall deformation of the CBS creates a vase-like shape caused by bending along the orthoradial axis (Figure 5a). In this FEM, local damage forms initially from the *intrinsic* irradiation-induced damage before being supplanted by the *structural* damage.

4. With increasing operation and the resulting increase in fluence, damage penetrates gradually through the CBS from its inner surface. At 40, 60, and 80 years of operation, damage depth reaches about 6, 9, and 11 cm, respectively. The damage extents are in agreement in the FEMs and LDPMs.

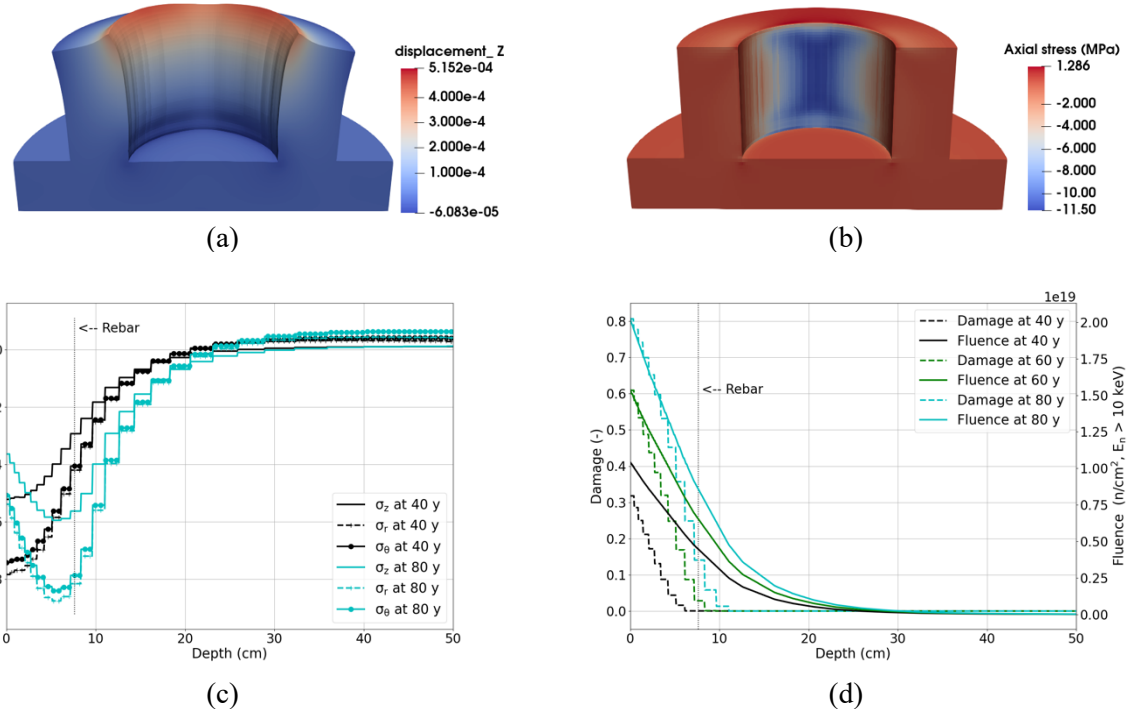

Figure 5. (a) Axial displacement shown on a distorted mesh (magnification ×1, 500, color bar unit in meters.); (b) vertical stresses at 80 years of operation; (c) radial profiles of radial, orthoradial and vertical stresses at 40 and 80 years of operation; and (d) radial profiles of damage at 40, 60 and 80 years of operation.

CONDITIONS DURING LOSS-OF-COOLANT ACCIDENT

The thermophysical behavior of the surface of the RPV and CBS during the large break loss-of-coolant accident (LBLOCA) of a PWR may change as a result of flow of the superheated steam released from the pipe rupture (e.g., double-ended guillotine break [DEGB]) through the air gap between the RPV and CBS. Most of the steam from the break at the cold leg will be released into the reactor containment dome, and some may flow through the air gap and RPV cavity. During this sequence, the CBS surface may be heated. RELAP5-3D, the model developed by Idaho National Laboratory (INL) for the nuclear system safety analysis code is used. This code can model a full-scale multi-dimensional nuclear power plant including the reactor core, steam generators, pumps, valves, accumulator, pressurizer, and pipes for both steady-state normal operation and various transients.

This study focuses on developing a methodological approach aimed at estimating the additional thermal damage caused by the LOCA-induced temperature increase of the air in the reactor cavity. Note that the dynamic loading effects (thrust force and differential pressure – See NUREG-0609 caused by pipe rupture are not considered in this preliminary study. The amount of steam through the air gap and cavity was assumed conservatively (e.g., 5–30% of total steam) to override unknown information on air gap opening geometry and the steam amount passing through, as shown on the left of Figure 6.

The INL Generic PWR (IGPWR) RELAP5-3D model – 2 GWth 3-loop Westinghouse – was originally used to assess the safety margin and plant damage during station blackout analyses and for natural hazard analyses in various LWRS projects. The model has been fully validated by steady-state and various transient calculations. The right side of Figure 6 shows the nodalization of IGPWR for RELAP5-3D

analysis, including 215 hydraulic volumes connected with 257 junctions, coupled with 240 heat structures to simulate heat generation and loss. In all heat structures, 1,312 mesh points are discretized in all heat structures. For the radial reactor core, three independent thermal-hydraulic channels are modeled to represent the central (volume 111), middle (volume 112) and periphery of the reactor core (volume 113 and 118). Passive and active heat structures simulate the heat transfer between the coolant and the fuel, the structures, and the secondary side of the IGPWR. The reactor core bypass (i.e., downcomer or belt line region) is modeled in volume 104 with no heat losses toward the containment, as in adiabatic insulation. Reactor core is linked with three identical steam generator loops. The following components are modeled: RPV; three reactor coolant loops (MCC), including the main coolant pumps (MCPs) and the steam generators (SGs); the pressurizer (PRZ) and its main valves (i.e., pilot-operated relief valve [PORV] and safety valve – [SV]); connections for the emergency core cooling system (ECCS) and auxiliary feed water system (AFWS); the secondary part of the SGs up to the SG outlet, including the SG main valves (PORV and SV); the main feed water (MFW); and the ECCS, including high- and low-pressure safety injection (HPSI and LPSI) systems and accumulators.

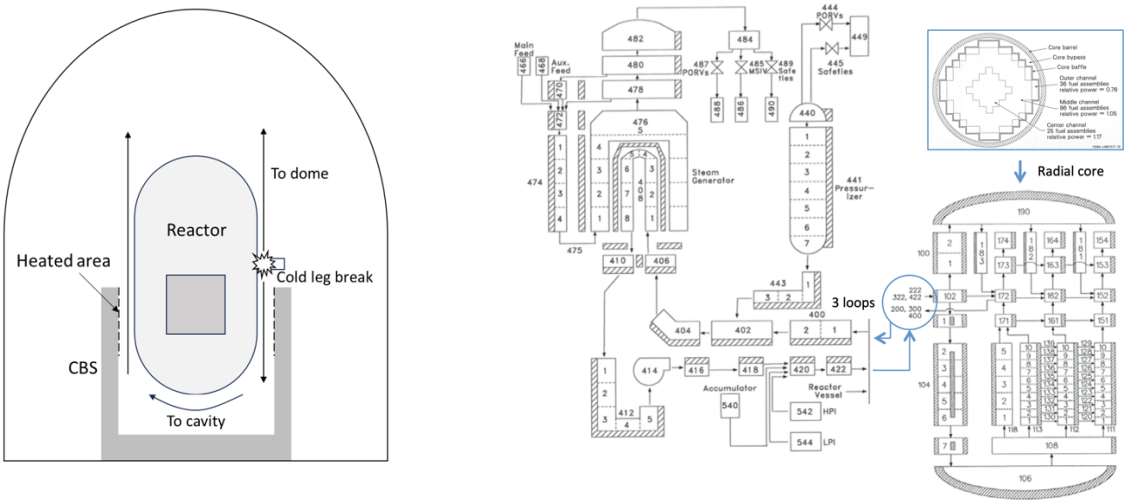

Figure 6. Schematic of the steam flow through the air gap (left), and RELAP5-3D nodalization for IGPWR (right).

Various scenarios were studied. With increasing mass flow rates, the air gap pressure increases more rapidly: with a mass flow of 1,800 kg.s^{-1}, the peak temperature of 370 K (~97 °C) is reached in approximately 30 seconds when the initial temperature in the air gap is 318 K (45 °C). The peak value is approximately 380 K (~107 °C) when the initial temperature in the air gap is 339 K (~66 °C). The air pressure derived from RELAP 5 simulations rapidly increases from 0.071 MPa in operation to reach approximately 0.275 MPa in about 10 s, and it decreases rapidly to return to the operating conditions as a result of the action of the spray cooling system in the containment. At the maximum increase of internal pressure and considering the dimensions of the CBS, the maximum stresses in the concrete are < 0.4 MPa in the orthoradial and vertical directions. In this example, these stresses are well below the tensile strength of the concrete and are one order of magnitude below the residual compressive stresses caused by restrained RIVEs. Thus, this study did not consider how the LBLOCA-induced air pressure increase applied to the surface of the CBS contributes to the formation of mechanical stresses. However, for plant specific evaluation, LBLOCA-induced degradation due to pressure should be taken into consideration.

LOCA-INDUCED DEGRADATION DUE TO THERMAL SHOCK

An LDPM-based sector model similar to that presented above is used to model the effects of an LBLOCA (reduction of the MSMD thickness to 300 mm). The preliminary study presented here is a plant with neutron

shield tank and limited to the effects of additional LOCA-induced thermal expansion. At this stage of the work, water vaporization-induced pressure and secondary limitations of the effects of cracking on the thermal properties of the concrete are not taken into account.

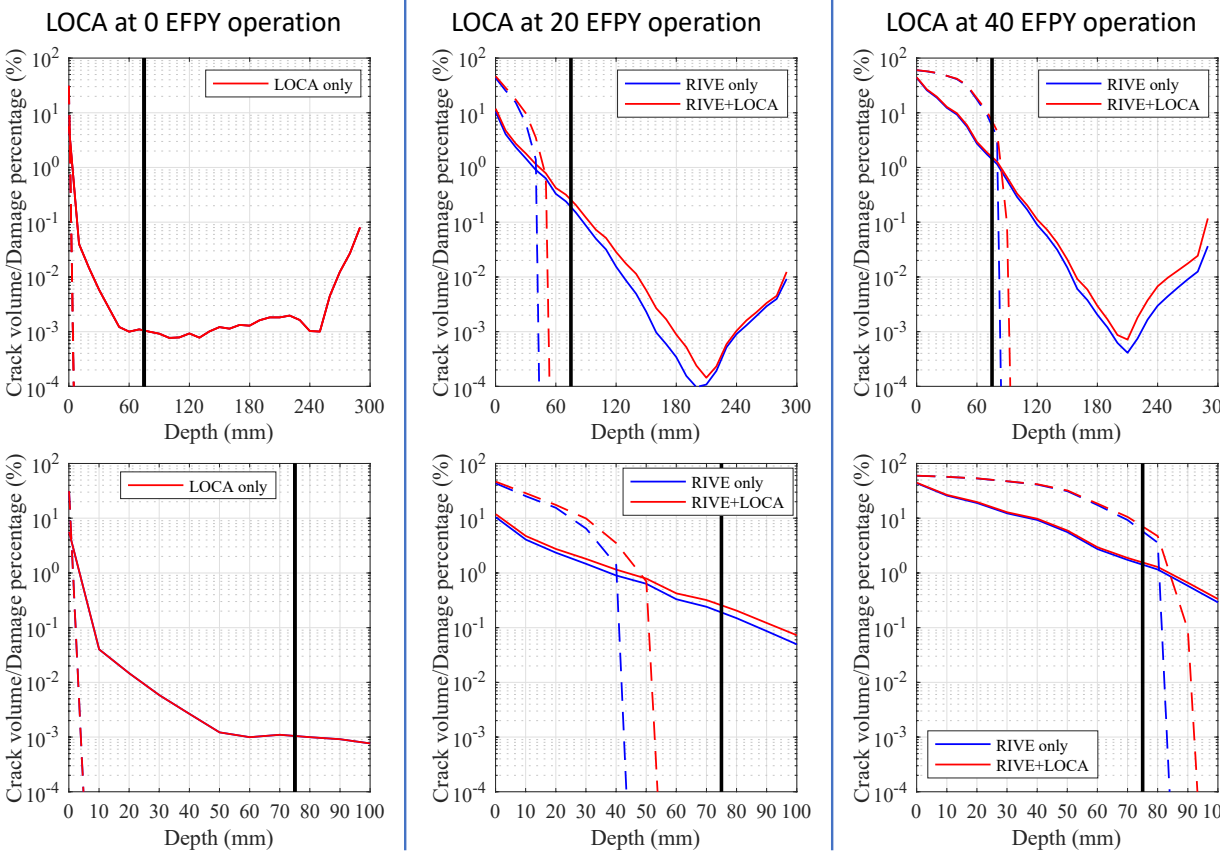

Figure 7. Crack volume (solid lines) and mechanical damage (dashed lines) radial profiles in the CBS caused by in-service irradiation (blue lines) and LOCA (red lines): LOCA occurring at 0 (left), 20 (center), and 40 (right) years of effective full power operation. The bottom figures are close-up profiles ranging from 0 to 10 cm.

The main results are presented in Figure 7. During a LOCA, the thermal shock applied to the CBS surface diffuses gradually inside the wall. The temperature increase in that region causes expansion. Qualitatively, this mechanism is comparable to RIVE, producing comparable effects such as vertical and orthoradial stresses. Because the radial profile gradients of fast neutron fluence and temperature are different, restrained RIVE and thermal expansions produce different damage profiles. After 20 and 40 years of effective full power operation, the LOCA-induced thermal expansion causes an increased damage depth of approximately 10 mm. It is notable that at 40 effective full power years of operation, the damage depth reaches extents of about 15 mm beyond the location (center) of the reinforcements. Degradation depth will depend on accumulated fluence, gamma dose, composition of aggregates, and other factors.

CONCLUSIONS

In this study, two different simulations methods, namely the FEM and LDPM, are used to assess the effects of in-service irradiation-induced degradation assuming that the irradiated properties of concrete obtained from test reactors data at higher fast neutron flux are applicable to light water reactors' irradiation conditions. The FEM and the LDPM on in-service irradiation-induced degradation are qualitatively in agreement for studied operational conditions (i.e., fast neutron fluence up to 2×10^{19} n.cm^{-2} (E > 10 keV)

at 80 years of operation), a temperature < 65 °C and a 92%-quartz content aggregate. In the concrete region near the reactor cavity, cracks open in the radial direction as a result of the vertical and orthoradial stresses caused by structural constraints. Larger cracks and thus more significant damage occurs near the reactor's cavity surface. Crack opening decreases, and thus damage decreases in relation to the distance from the reactor cavity surface. Damage depth extends beyond the concrete region subject to fast neutron fluence $> 10^{19}$ n.cm^{-2} (E>10 keV). Quantitatively, the radial damage profile is different from the two models. Whereas damage penetrations are comparable between the FE and LDPM simulations, the LDPM shows that there is no substantial bearing capacity in the concrete near the reactor cavity. For engineering calculation purposes using FE simulation, it is suggested to assume that the compressive strength of concrete between the reactor cavity and the irradiation-induced damaged depth is negligible. During the studied LOCA conditions, the thermal expansion of the concrete caused by the temperature increase in the reactor cavity results is a minor increase of the depth of degradation on the CBS under the modelled conditions. For plant specific evaluation, LBLOCA-induced degradation due to pressure and thermal expansion of the concrete should be considered in addition to degradation due to radiation. This methodological study is provided as a demonstration only. Refer to NUREG/CR-7280 and NUREG/CR-7281 for the additional information on CBS design and irradiation transport model.

ACKNOWLEDGMENTS

This research was sponsored by the US Department of Energy (DOE) Office of Nuclear Energy Light Water Reactor Sustainability Program Materials Research Pathway under contract DE-AC05-00OR22725 with UT Battelle LLC/Oak Ridge National Laboratory (ORNL).

NOTICE OF COPYRIGHT

REFERENCES

Avramova, M. N. (2009). CTF: A *Thermal Hydraulic Sub-Channel Code for LWR Transient Analyses, User's Manual*. Technical Report, Pennsylvania State University Department of Nuclear Engineering.

Bažant, Ž. P. and Jirásek (2018). "Creep and hygrothermal effects in concrete structures," Vol. 225 of *Solid Mechanics and Its Applications*, Springer.

Cheniour, A., et al. (2023). "A structural model of the long-term degradation of the concrete biological shield," *Nuclear Engineering and Design*, 405:112217.

Collins, B., et al. (2016). *MPACT VERA Input User's Manual Version 2.2.0*. Technical Report CASL-U-2016-1109-000, CASL.

Cusatis, G., Pelessone, D. and Mencarelli, A. (2011). "Lattice Discrete Particle Model (LDPM) for Concrete Failure Behavior of Concrete. I: Theory." *Cement and Concrete Composites*, 33(9):881–890.

Denisov, A. V., Dubrovskii, V. B., and Solovyov, V. N. (2012). *Radiation Resistance of Mineral and Polymer Construction Materials*, ZAO MEI Publishing House.

Esselman, T. and Bruck, P. (2018). *Expected Condition of Concrete Exposed to Radiation at Age 80 Years of Reactor Operation*, ORNL/TM-2018/769, Oak Ridge National Laboratory.

Field, K. G., Remec, I. and Le Pape, Y. (2015). "Radiation effects on concrete for nuclear power plants – Part I: Quantification of radiation exposure and radiation effects," *Nuclear Engineering and Design*, 282:126–143.

Godfrey, A. T., et al. (2016). "*VERA Benchmarking Results for Watts Bar Nuclear Plant Unit 1 Cycles 1-12*. Technical Report CASL-U-2015-0206-000, CASL.

Hilsdorf, H. K., Kropp, J., and Koch, H. J. (1978). "The effects of nuclear radiation on the mechanical properties of concrete," *Special Publication of The American Concrete Institute*, 55:223–254.

Kambayashi, D., Sasano H., Sawada, S., Suzuki, K. and Maruyama, I. (2020). "Numerical analysis of a concrete biological shielding wall under neutron irradiation by 3D RBSM," *Journal of Advanced Concrete Technology*, 18:617-632.

Kochunas, B., et al. (2017). "VERA Core simulator methodology for PWR cycle depletion," *Nuclear Science and Engineering*, 186:217–231.

NUREG/CR-0609, "Asymmetric Blowdown Loads on PWR Primary Systems – Resolution of Generic Task Action Plan A-2, Report November 1980, January 1981, https://www.nrc.gov/reading-rm/doc-collections/nuregs/staff/sr0609/index.html

NUREG/CR-7280, "Review of Radiation Induced Concrete Degradation and Potential Implications for Structures Exposed to High, Long-Term Radiation Levels in Nuclear Power Plants," Report December 2020, published July 2021, https://www.nrc.gov/reading-rm/doc-collections/nuregs/contract/cr7280/index.html

NUREG/CR-7281, "Radiation Evaluation Methodology for Concrete Structures," Report December 2020, published July 2021, https://www.nrc.gov/reading-rm/doc-collections/nuregs/contract/cr7281/index.html

Permann, C. J. et al. (2020) "MOOSE: Enabling massively parallel multiphysics simulation." *SoftwareX*, 11:100430.